IOP SHORT MEETINGS

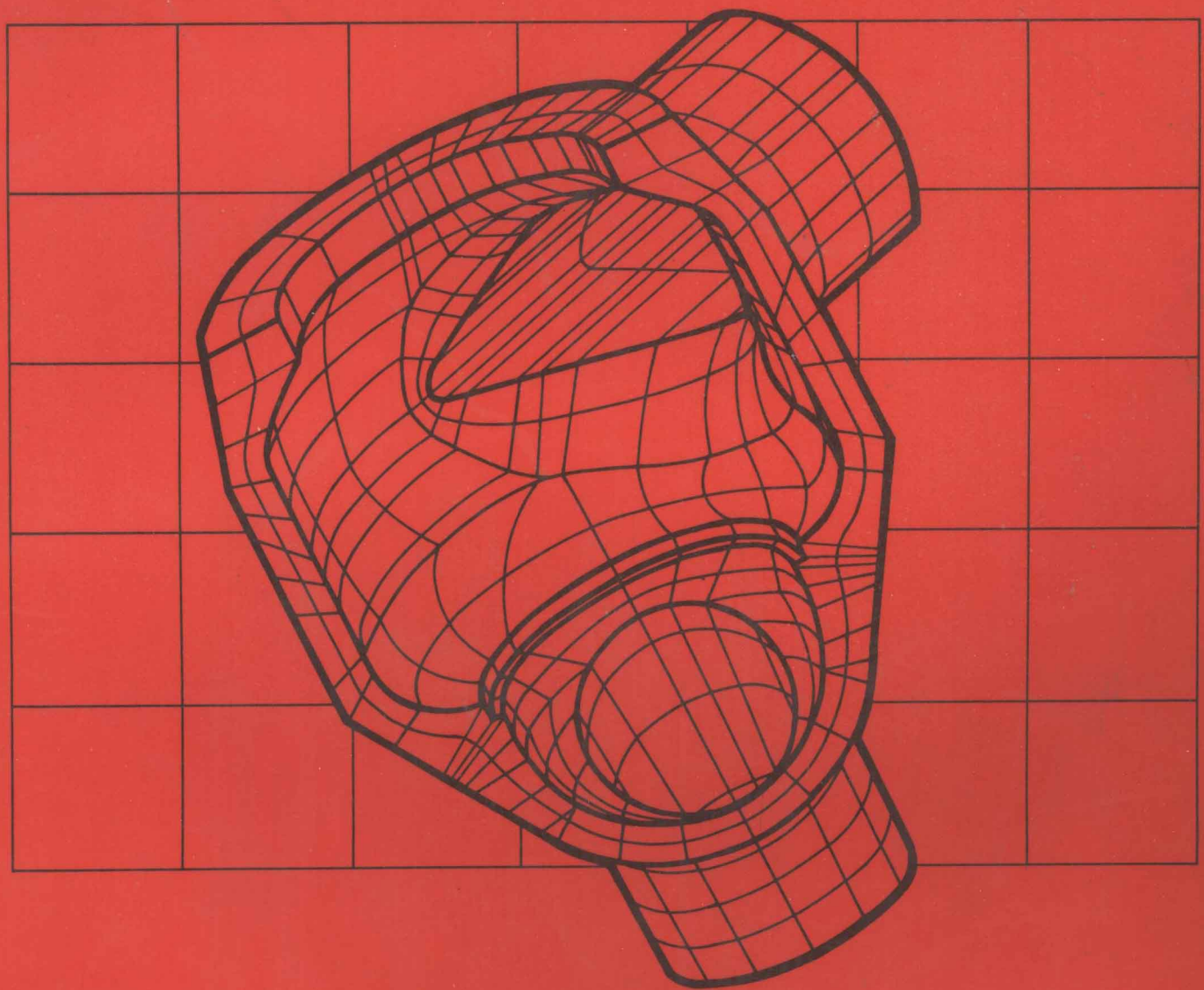

BOUNDARY ELEMENT METHODS

THEORY & APPLICATION

BOUNDARY ELEMENT METHODS

Theory and Application

A meeting of the Stress Analysis Group
of the Institute of Physics
4th July 1986
LONDON

IOP Short Meeting Series No 1
Institute of Physics

CODEN — IPS SE3

British Library Cataloguing in Publication Data

Boundary element methods: theory and application. — (IOP short meetings series; no. 1) 1. Strains and stresses 2. Boundary value problems
I. Series
620.1'123'01515353 TA407

ISBN 0 85498 500 X
ISSN 0269 0896

Published by The Institute of Physics
Techno House, Redcliffe Way, Bristol BS1 6NX, England

Printed in Great Britain by Gibbons Barford Print, Wolverhampton

Contents

The Boundary Element Method for Stress Concentration and Fracture Problems

S. Ellis, R.N.L. Smith and J.C. Mason

Computational Mathematics Group, Royal Military College of Science, Shrivenham, Swindon, Wiltshire

Abstract

An implementation of the boundary element method for two-dimensional elasticity and fracture problems is described, and results for of stress concentration, and straight and curved crack problems are given. A transformation of a body force integral to a boundary representation is presented and an example of it's use with a crack problem is illustrated.

1 Introduction

The boundary element method (BEM) is now established as a powerful tool for the solution of linear partial differrential equations. In particular, elliptic problems such as those arising in potential theory or elasticity have proved to be especially suited to the BEM approach.

For the solution of stress or fracture problems, the BEM is likely to be superior to other general methods such as the finite element method (FEM) in a number of ways. Since only the boundaries of a body need to be discretized, very much smaller systems of equations are generated than with the FEM. (Whilst smaller, they are in general fully populated. However, provided the ratio of the boundary length to area is not excessive, boundary methods retain their superiority.) As no internal approximation is made, a higher stress accuracy is achieved, values of solution variables are obtained at a limited number of points, and it is possible to concentrate on particular regions of interest (e.g. stress concentrations, cracks and interfaces). The superiority of the BEM is particularly marked for those problems where the boundary stresses change rapidly as in stress concentration and fracture problems.

The technique involves superposition of particular solutions of the governing differential equations. In the direct integral equation formulation the unknown functions are the physical stresses and displacements on the boundaries, and the basic analytical solutions used are those for a unit force applied to an infinite region in which the physical region is 'embedded'. A summary of the derivation of the integral equation for two-dimensional elasticity is presented, followed by a description of our numerical implementation of the BEM for this equation.

A typical stress concentration problem is that of plates of differing widths joined by a simple curve and loaded under tension. The problem is modelled using our two-dimensional boundary element program with

isoparametric elements. The BEM solutions are compared with those obtained by photoelastic stress analysis with good agreement over a wide range of plate shapes.

The basic BEM formulation must be modified to deal with general fracture problems where cracks are to be modelled. The stresses at the tip of a sharp crack in a perfectly elastic region may be expressed in terms of an infinite series of the form

$$\sigma = K\, F(\theta)\, \sqrt{r} \;+\; \text{non-singular terms}$$

and the boundary elements should be modified to model this knwn behaviour. With suitably modified elements the accuracy of the BEM is much improved and both straight and curved cracks may be considered. We give examples of BEM solutions which demonstrate these points, and which compare favourably with established analytical and numerical results.

Some simple body forces such as rotational, gravitational or thermal loads may be transformed into equivalent boundary forces. We give an example of this transformation for a crack problem and discuss two sets of finite element results for the same problem.

2 Integral equation formulation

The formulation of the direct method, which is summarised below, follows the approach used by Lachat and Watson |11| , and it is restricted to two-dimensional homogeneous linearly elastic regions. As is customary vectors such as points x and y are not underlined and tensor notation is adopted.

Fundamental solutions for displacements $U_{ij}(x,y)$ and tractions $T_{ij}(x,y)$, are determined from the governing equations for a point force in an infinite elastic space

$$\frac{\partial \sigma_{kj}}{\partial x_k} + \delta_i = 0 \tag{2.1}$$

and are found to be

$$U_{ij}(x,y) = \frac{1}{8\pi(1-\nu)} \left[(3-4\nu)\, \ln(1/r)\, \delta_{ij} + r_{,i} r_{,j} \right] \tag{2.2}$$

$$T_{ij}(x,y) = \frac{-1}{4\pi(1-\nu)} \frac{1}{r} \left[\frac{r}{n} \left(k\, \delta_{ij} + 2 r_{,i} r_{,j} \right) + k\left(r_{,j} n_i - r_{,i} n_j \right) \right]$$

where , are elastic constants, $n_i = n_i(x)$ is the outward normal to R at x, and

$$r = (x_i - y_i)\,(x_i - y_i)^{1/2}$$

$$r_{,i} = \frac{\partial r}{\partial x_i} = \frac{1}{r}(x_i - y_i) \tag{2.3a}$$

$$\frac{\partial r}{\partial n} = \frac{\partial r}{\partial x_i} n_i = \frac{1}{r}(x_i - y_i)n_i$$

$$k = (1-2\nu) \qquad (2.3b)$$

The traction $t_i(x)$ on the tangent plane corresponding to the complementary function $u_i(x)$, is given by

$$t_i(x) = \sigma_{ij}[u] \; n_j(x) \qquad (2.4)$$

The boundary integral equation may now be derived using the divergence theorem :

$$\int_V \frac{\partial c_s(y)}{\partial y_s} \, dV_y = \int_S n_s(y) c_s(y) \, dS_y \qquad (2.5)$$

We now consider the displacement fields $a_s(y)$ and $b_s(y)$. In equation (2.5), $c_s(y)$ may be replaced by $b_j(y)\sigma_{js}[a]$, then by $a_j(y)\sigma_{js}[b]$, and one of the resulting equations subtracted from the other. This process gives the equation

$$\int_V \left[b_j(y) \frac{\partial \sigma_{js}}{\partial y_s}[a] - a_j(y) \frac{\partial \sigma_{js}}{\partial y_s}[b] \right] dV_y$$

$$= \int_S \left[b_j(y) \sigma_{js}[a] - a_j(y) \sigma_{js}[b] \; n_s(y) \right] dS_y \qquad (2.6)$$

which is known as Betti's theorem and is analogous to Green's symmetric identity for the Laplace operator. Replacing $a_j(y)$ by $u_j(y)$, and $b_j(y)$ by $U_{ij}(x,y)$ (for x on S), noting that for a source free region $\partial\sigma_{ij}/\partial x^j = 0$, and taking for V the region $R' = R - R_e$ where R_e isolates the point x, we obtain:

$$\int_{S'} \left[U_{ij}(x,y) \; t_j(y) - T_{ij}(x,y) \; u_j(y) \right] dS_y = \int_{V'} U_{ij}(x,y) \; b_i(y) \; dV_y \qquad (2.7)$$

Here R_e is conventionally taken to be the part of R contained within a sphere of radius e, centre x. Hence, by letting $e \to 0$, with x on S, we obtain

$$c_{ij}(x) \; u_j(x) + \int_S T_{ij}(x,y) \; u_j(y) \, dS_y = \int_S U_{ij}(x,y) \; t_j(y) \, dS_y + \int_V U_{ij}(x,y) \; b_i(y) \, dV_y \qquad (2.8)$$

where

$$c_{ij}(x) = \lim_{e \to 0} \int_{S_e} T_{ij}(x,y) \, dS_y$$

If the target plane is continuous at x, then $c_{ij}(x) = 1/2 \, \delta_{ij}$. An expression for the displacement may be obtained from Betti's theorem by a similar limiting process in the form

$$u_i(x) = \int_S U_{ij}(x,y)\, t_y(y)\, dS_y - \int_S T_{ij}(x,y)\, u_j(y)\, dS_y + \int_V U_{ij}(x,y)\, b_i(y)\, dV_y \qquad (2.9)$$

The corresponding expression for the stress tensor at an interior point is

$$\sigma_{ij}(x) = \int_S D_{ijs}(x,y)\, t_s(y)\, dS_y - \int_S S_{ij}(x,y)\, u_s(y)\, dS_y + \int_V D_{ijs}(x,y)\, b_s(y)\, dV_y \qquad (2.10)$$

where $D_{ijs} = \sigma_{ij}\,|U|$ and $S_{ijs} = \sigma_{ij}\,|T|$.

3 Numerical implementation

We assume for the moment that body forces are not present. Their inclusion will be dealt with in section 5.

The boundary S is partitioned, into N_e boundary elements (Figure 3.1), and the integral equation becomes

$$c_{ij}(x)\, u_j(x) + \sum_{k=1}^{N_e} \int_S T_{ij}(x,y)\, u_j^k(x,y)\, dS_y = \sum_{k=1}^{N_e} \int_S U_{ij}(x,y)\, t_j^k(y)\, dS_y \qquad (3.1)$$

where u_j^k, t_j^k represent the j^{th} components of displacement and traction on the k^{th} element.

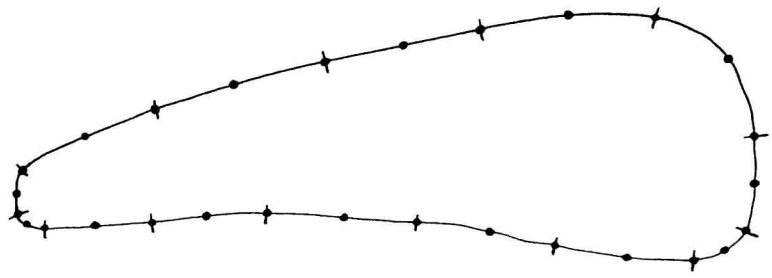

Figure 3.1 Boundary mesh

On each element the boundary, displacement and traction are assumed to vary in some simple fashion. Variations are represented by discrete values at nodes, and basis (or shape) functions are used to obtain a piecewise approximation. The boundary representation must be piecewise continuous, and it should also be a reasonable approximation to the true boundary. However the displacements and tractions may be discontinuous, and so the geometry and unknown functions may use different shape functions, with nodes at different positions. In practice it is simpler to use isoparametric elements in which the same shape functions and nodal positions are used. Typically m+1 equally spaced nodes are placed on each element, and an m^{th} degree polynomial approximation is adopted.

We use quadratic elements (m=2), which allow the modelling of curved boundaries, and which may be easily modified to allow representation of certain singularities (see section 4).

We represent the cartesian coordinates x_j, and the unknowns u and t in terms of a local coordinate $\xi \in [0,1]$, in the form

$$\begin{bmatrix} x^j(\xi) \\ u(\xi) \\ t(\xi) \end{bmatrix} = \begin{bmatrix} x_j^1 & x_j^2 & x_j^3 \\ u^1 & u^2 & u^3 \\ t^1 & t^2 & t^3 \end{bmatrix} \begin{bmatrix} N^1(\xi) \\ N^2(\xi) \\ N^3(\xi) \end{bmatrix} \qquad (3.2)$$

where $N^i(\xi)$ are the shape functions (Figure 3.2), and the superscripts 1,2,3 denote the values of the coordinates and unknowns at ξ = 0, 1/2, 1. Specifically we write

$$\begin{aligned} N^1(\xi) &= 2(\xi - 1/2)(\xi - 1) \\ N^2(\xi) &= -4\,\xi\,(\xi - 1) \\ N^3(\xi) &= 2\,\xi\,(\xi - 1/2) \end{aligned} \qquad (3.3)$$

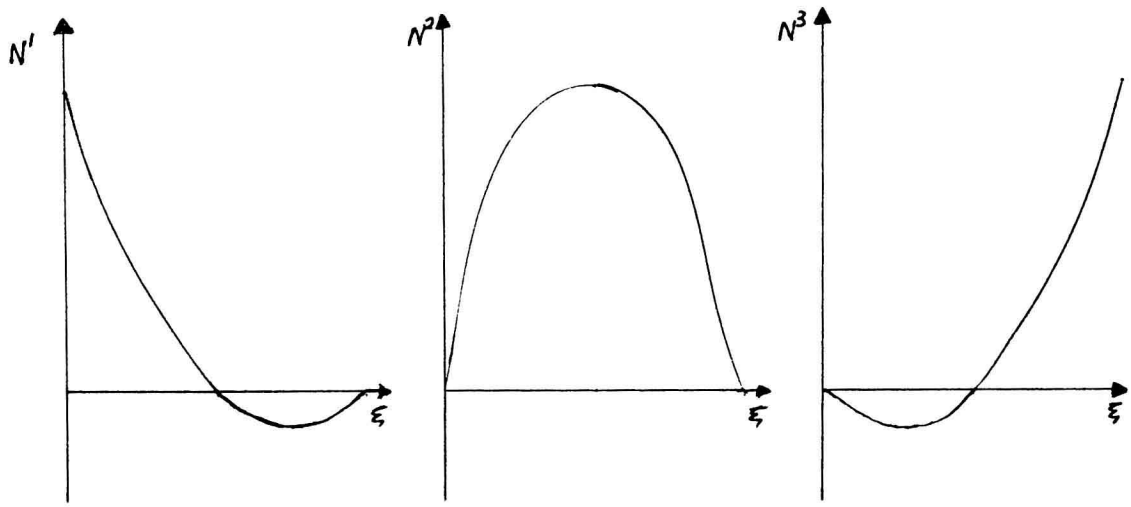

Figure 3.2 - Quadratic shape functions

Substituting these representations into the integral equation gives

$$c_{ij}(x)\, u_j(x) + \sum_{k=1}^{Ne} \int_0^1 \sum_{a=1}^{3} T_{ij}(x,y(\xi))\, M^a(\xi)\, u_j^{k,a}\, J(\xi)\, d\xi = \sum_{k=1}^{Ne} \int_0^1 \sum_{a=1}^{3} U_{ij}(x,y(\xi))\, M^a(\xi)\, t_j^{k,a}\, J(\xi)\, d\xi \tag{3.4}$$

where $J(\xi)$ is the Jacobian

$$J(\xi) = \left[\left(\sum_{a=1}^{3} dM^a(\xi)\, y_1^a \right)^2 + \left(\sum_{a=1}^{3} dM^a(\xi)\, y_2^a \right)^2 \right]^{1/2}$$

In matrix form the equation becomes

$$c(x)\, u(x) + \sum_{k=1}^{N} \sum_{a=1}^{3} p^{k,a}\, u^{k,a} = \sum_{k=1}^{N} \sum_{a=1}^{3} q^{k,a}\, t^{k,a} \tag{3.5}$$

where

$$c = \begin{bmatrix} c_{11} & c_{12} \\ c_{21} & c_{22} \end{bmatrix} \quad p = \begin{bmatrix} p_{11} & p_{12} \\ p_{21} & p_{22} \end{bmatrix} \quad q = \begin{bmatrix} q_{11} & q_{12} \\ q_{21} & q_{22} \end{bmatrix}$$

$$u = \begin{bmatrix} u_1 \\ u_2 \end{bmatrix} \quad \text{and} \quad t = \begin{bmatrix} t_1 \\ t_2 \end{bmatrix} \tag{3.6}$$

and

$$p_{ij} = \int_0^1 T_{ij}(x,y(\xi))\, M(\xi)\, J(\xi)\, d\xi$$

$$q_{ij} = \int_0^1 U_{ij}(x,y(\xi))\, M(\xi)\, J(\xi)\, d\xi \tag{3.7}$$

The analytical evaluation of the integrals (3.7) appears to be very difficult for quadratic elements with curved geometry. We therefore use Gauss quadrature formulae to obtain approximate values. An additional complication arises in the use of numerical methods owing to the presence of the term log(1/r) in the second integral. When the boundary point x is a node of the element being integrated over, r is zero at that node. The integral is therefore weakly singular at x. It can be shown (Smith [17]) that this integral can be written as

$$I_s = \int_0^1 \log(\xi)\, M^a(\xi)\, J(\xi)\, d\xi +$$

$$\frac{1}{2}\int_0^1 \log(A\xi^2 + B\xi + C)\, M^a(\xi)\, J(\xi)\, d\xi \qquad (3.8)$$

where the second integral does not contain a singularity for elements of modest size and curvature. The first integral is evaluated with weight function $\log(\xi)$, and the second integral with weight function 1. Numerical experiments indicate that integration rules of order 6 are sufficient for typical problems, and we use such rules in all subsequent examples.

If we consider the point x to be the m^{th} of N_n boundary nodes, then we may express (3.5) in terms of the coefficients for displacements and tractions at each node :

$$c_m u_m + \sum_{n=1}^{N_n} h_{mn} u_n = \sum_{n=1}^{N_n} g_{mn} t_n \qquad (3.9)$$

or $$(C + H)\, u = G\, t$$

Note that for nodes at the junction of two elements these coefficients include contributions from both elements, so that

$$\begin{aligned} h_{mn} &= p^{k-1,3} + p^{k,1} & g_{mn} &= q^{k-1,3} + q^{k,1} \\ h_{mn} &= p^{k,2} & g_{mn} &= q^{k,2} \\ h_{mn} &= p^{k,3} + p^{k+1,1} & g_{mn} &= q^{k,3} + q^{k+1,1} \end{aligned} \qquad (3.10)$$

are contributions to the three nodes in element k from elements k-1, k, and k+1.

The blocks c_m may be determined by considering rigid body motion. Suppose that unit rigid body translations occur in directions k, with zero applied tractions. Then

$$(C + H)\, L_k = 0$$

and the diagonal blocks must therefore be given by

$$(C + H)_{ii} = \sum_{\substack{j=1 \\ j \neq i}}^{R} h_{ij}$$

If we assume that tractions are continuous, then for each node we have two equations in four variables. Two of these are known, and the system of equations may be reordered with all the unknowns on the left hand side.

Discontinuous applied tractions are dealt with by constructing the right hand side using only the contributions to g_{mn} in (3.10) from the element on which each traction is applied. For discontinuous unknown tractions more equations must be generated and techniques dealing with

this problem are dealt with by Patterson and Sheikh |14|. The implementation above produces an "average" value, which for a large number of problems is adequate.

We solve the resulting system of equations, in most cases, using Gauss elimination. In some cases, when all boundary conditions are tractions the displacements include an arbitrary rigid body displacement. If at least two equations are replaced by equations specifying displacements at particular nodes this difficulty is overcome. Alternatively, the existing system of equations may be solved in a least squares sense.

Stresses are calculated using derivatives of the calculated displacements. The stresses are discontinuous across element boundaries, and a simple smoothing technique is employed to yield continuous values. The displacement derivatives are averaged at element boundaries and these average values are used to evaluate the stresses.

3.1 Example 1 - Stress concentrations in shouldered plates

The effect of changes in boundary shape on surface stresses is characterised by the stress concentration factor, which may be used subsequently to estimate the likelihood of crack formation. Values of stress concentration factors K_t for a range of commonly used used shapes are given by Peterson |15| , who defines K_t as

$$K_t = \sigma_{max} / \sigma_{nom}$$

where σ_{max} is the maximum stress in the region under consideration and σ_{nom} is the nominal applied stress.

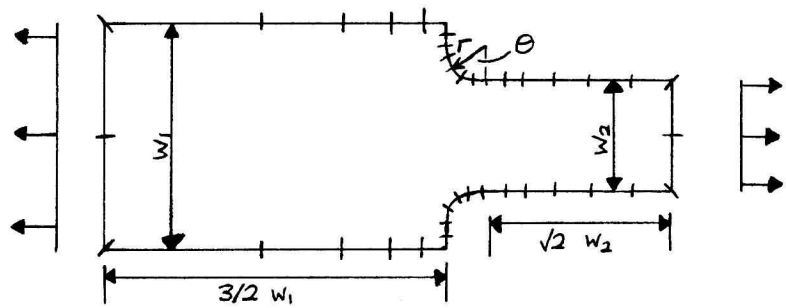

Figure 3.3 - Boundary element mesh for a shouldered plate

The problem of determining stress concentration factors for plates of differing widths joined by a part-circular arc is examined in a number of publications. For example Fessler et al |9| and Wilson and White |23| use photoelastic techniques to examine the variation of boundary stresses and determine stress concentration factors. We use our BEM to compare the stress variation in shouldered plates with that obtained by photoelastic analysis. A typical boundary element mesh is shown in Figure 3.3, and the stress variations obtained for two examples of corner radii are plotted in Figure 3.4.

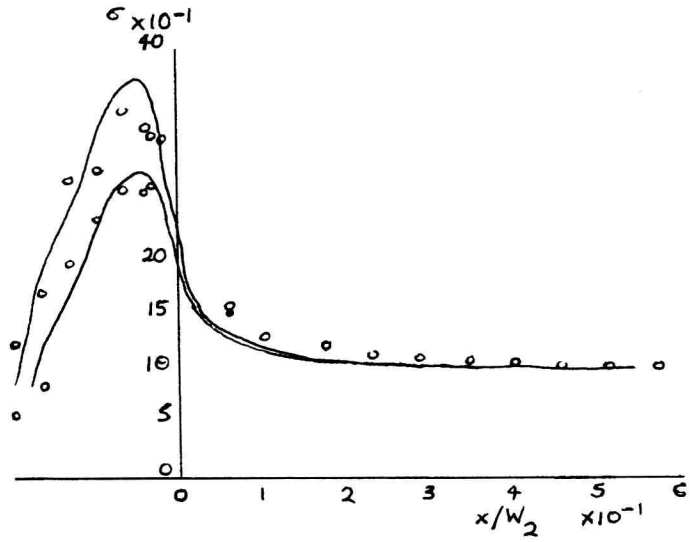

Figure 3.4 - Stress variation on a plate boundary (w1/w2 = 2.0)

The BEM results are shown by the full lines, and the results of Fessler et al are plotted point by point. The amount of scatter in the experimental results makes it difficult to draw a smooth curve and determine the maximum values exactly. In contrast, the BEM values form smooth curves with well determined maxima. The higher of the two peaks in Figure 3.4 corresponds to the case r/w = 0.036 for which Fessler et al obtain K_t = 3.7 at θ= 30°, and the BEM curve gives K_t = 3.7 at θ = 23.5°. Although there is apparently a significant difference between the two methods, the BEM curve is reasonably consistent with the experimental results given the amount of scatter therein. The lower peak in Figure 3.4 corresponds to r/w = 2.8 with K_t = 2.7 at θ = 22° (Fessler), K_t = 2.8 at θ= 21° (BEM). Agreement between the two methods may therefore be considered satisfactory, although further comparisons would be useful.

An extension to these problems is investigated by Smith and Crook |18| who examine problems with cracks at the reentrant corners of shouldered plates.

4 Linear elastic fracture and crack modelling

Linear elastic fracture mechanics assumes perfectly elastic regions and does not consider effects such as plasticity in the crack tip region. Nevertheless results obtained by the application of a linear model are widely adopted as reliable indicators of maximum stress levels and hence predictors of possible crack growth.

In two dimensions we consider two possible independent movements of the crack surface. They are the crack opening mode (mode I), and the crack sliding mode (mode II). These two modes are illustrated in Figure 4.1 below.

Conventionally, crack tip behaviour is expressed in an infinite series expansion due to Williams |22|. Series in increasing powers of displacements corresponding to the two modes may be derived via suitable stress functions (Paris and Sih |13|), and the first non-zero

terms in each series is given below.

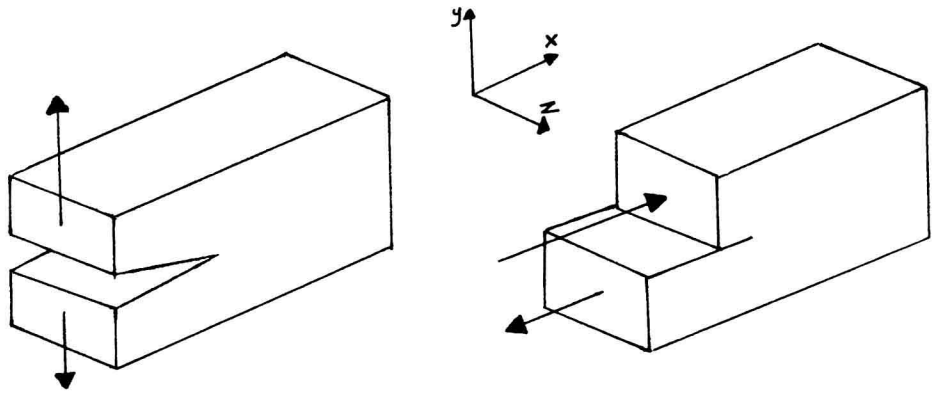

(a) Mode I displacement (b) Mode II displacement

Figure 4.1 - Two dimensional fracture modes

Mode I

$$\sigma_x = \frac{K_I}{\sqrt{2\pi r}} \cos\frac{\theta}{2}\left[1 - \sin\frac{\theta}{2}\sin\frac{3\theta}{2}\right] + \ldots$$

$$\sigma_y = \frac{K_I}{\sqrt{2\pi r}} \cos\frac{\theta}{2}\left[1 + \sin\frac{\theta}{2}\sin\frac{3\theta}{2}\right] + \ldots$$

$$\tau_{xy} = \frac{K_I}{\sqrt{2\pi r}} \sin\frac{\theta}{2}\cos\frac{\theta}{2}\cos\frac{3\theta}{2} + \ldots \qquad (4.1)$$

$$u = \frac{K_I}{4\mu}\sqrt{\frac{r}{2\pi}}\left[(2\kappa - 1)\cos\frac{\theta}{2} - \cos\frac{3\theta}{2}\right] + \ldots$$

$$v = \frac{K_I}{4\mu}\sqrt{\frac{r}{2\pi}}\left[(2\kappa + 1)\sin\frac{\theta}{2} - \sin\frac{3\theta}{2}\right] + \ldots$$

where $$K_I = \sqrt{2\pi r}\lim_{r\to 0}\sigma_y$$

Mode II

$$\sigma_x = -\frac{K_{II}}{\sqrt{2\pi r}} \sin\frac{\theta}{2}\left[2 + \cos\frac{\theta}{2}\cos\frac{3\theta}{2}\right] + \ldots$$

$$\sigma_y = \frac{K_{II}}{\sqrt{2\pi r}} \sin\frac{\theta}{2}\cos\frac{\theta}{2}\cos\frac{3\theta}{2} + \ldots$$

$$\tau_{xy} = \frac{K_{II}}{\sqrt{2\pi r}} \cos\frac{\theta}{2}\left[1 - \sin\frac{\theta}{2}\sin\frac{3\theta}{2}\right] + \ldots \qquad (4.2)$$

$$u = \frac{K_{II}}{4\mu}\sqrt{\frac{r}{2\pi}}\left[(2\kappa + 3)\sin\frac{\theta}{2} + \sin\frac{3\theta}{2}\right] + \ldots$$

$$v = \frac{K_{II}}{4\mu}\sqrt{\frac{r}{2\pi}}\left[(2\kappa - 3)\cos\frac{\theta}{2} - \cos\frac{3\theta}{2}\right] + \ldots$$

where $K_{II} = \sqrt{2\pi r} \lim_{r \to 0} \tau_{xy}$

Here κ is the shear modulus and μ is $(3 + \nu)$ for plane strain, and $(3 - \nu)(1 + \nu)$ for plane stress.

The crack tip geometry is defined in figure 4.2.

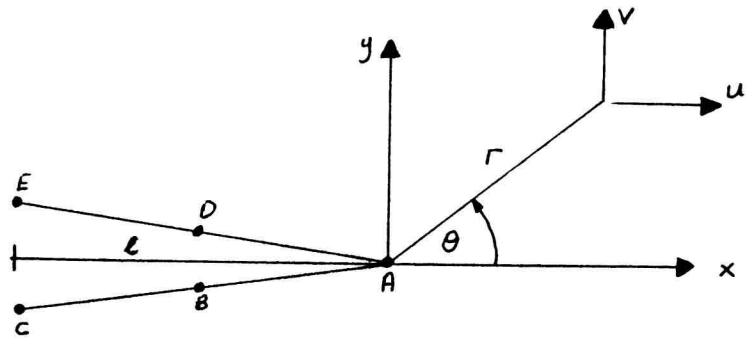

Figure 4.2 - Crack tip geometry

K_I and K_{II} define the magnitude of the crack tip stress field singularity, and are termed stress intensity factors (SIFs). They are important parameters, and connect with fracture theory through the postulate that a crack will grow when the SIFs reach particular values.

An idealised crack configuration (where both surfaces lie in the same plane) involves a surface discontinuity. Application of the standard direct BEM to such a configuration produces a singular algebraic system which contains no information about the crack surface, since the method cannot distinguish between two surfaces in the same plane. Crack geometries were initially approximated by seperating the surfaces some small distance. This crude approach leads to results of rather limited accuracy.

However, if the problem happens to be symmetric about the crack, then only one region and hence only one side of the crack needs to be considered, and the resulting linear algebraic system contains the relevant information, and may be solved successfully (Cruse |4|).

For some special cases, a Green's function is available, and then the fundamental solutions may be determined for a crack or a hole in an infinite region. Once these modified solutions have been incorporated into the integral equation, only the non-cracked boundary may be be modelled. Very accurate results are possible with this approach (Snyder and Cruse |23|).

We have adopted the more general technique of "stitching", which permits the two sides of the crack surface to be assigned to distinct subregions. This appears to overcome problems encountered by other methods and has been used eith success on a number of problems (Blandford et al |1|). The domain is partitioned so as to differentiate between pairs of crack surfaces, effectively introducing

additional boundaries internal to the domain (Figure 4.3). Continuity conditions are imposed across partitions, but not of course across cracks. The geometry of the crack may be represented accurately, whether or not the crack is on a plane of symmetry, and also curved cracks may be modelled.

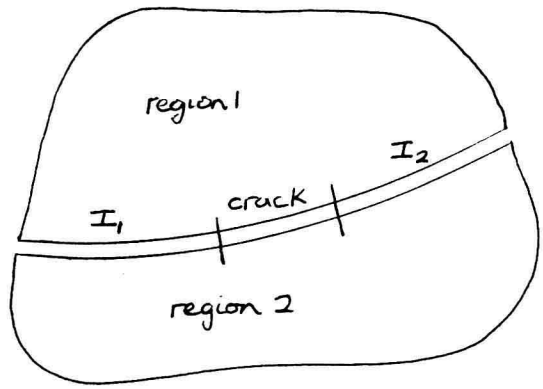

Figure 4.3 - Stitching subregions

Interface conditions are applied by coupling the systems of equations generated for each subregion, effectively treating the subregions as large finite elements. Across the interface the displacements u_j are continuous, while the tractions t_j are equal in modulus but have opposite signs. Consider the example of two subregions as in Figure 4.2. The systems of equations generated may be written as

$$\begin{bmatrix} H_1 & H_1^I & G_1^I \end{bmatrix} \begin{bmatrix} u_1 \\ u_1^I \\ t_1^I \end{bmatrix} = \begin{bmatrix} G_1 \end{bmatrix} \begin{bmatrix} t_1 \end{bmatrix} \qquad \begin{bmatrix} H_2 & G_2 & H_2 \end{bmatrix} \begin{bmatrix} u_2 \\ t_2^I \\ u_2^I \end{bmatrix} = \begin{bmatrix} G_2 \end{bmatrix} \begin{bmatrix} t_2 \end{bmatrix}$$

where the superscript I denotes interface values. Applying the continuity conditions

$$u_1^I = u_2^I = u^I, \text{ and } t_1^I = -t_2^I = t^I$$

and combining the equations, gives

$$\begin{bmatrix} H_1 & H_1^I & G_1^I & 0 \\ 0 & H_2^I & -G_2^I & H_2 \end{bmatrix} \begin{bmatrix} u_1 \\ u^I \\ t^I \\ u_2 \end{bmatrix} = \begin{bmatrix} G_1 & 0 \\ 0 & G_2 \end{bmatrix} \begin{bmatrix} t_1 \\ t_2 \end{bmatrix} \tag{4.3}$$

Boundary conditions are applied as in section 3 to produce a system of

linear algebraic equations. This system differs from the first in that sections of the coefficient matrix are now empty. In most problems we deal with the matrix is actually block-banded, and this knowledge can be used to increase the efficiency of our equation solver. Stresses are sampled in exactly the same manner as for a single subregion.

The equations (4.1) and (4.2) show that,when r is small, the stresses behave as $r^{-1/2}$ (within the material) and the displacements behave as $r^{1/2}$. It has been found advantageous to model the known behaviour near the crack tip (see example 2). Modelling of the $r^{1/2}$ term can be effectively achieved by using quarter-point elements, in which the mid point node on a quadratic element is moved to $\xi = 1/4$ (Figure 4.4).

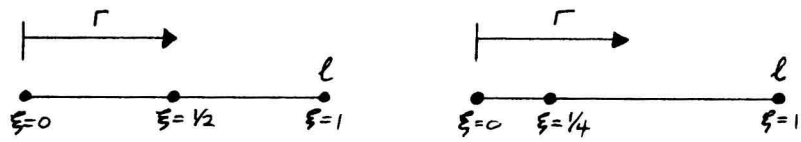

Figure 4.4 - Quarter-point element

For the quarter-point element, r is equivalent to l^2, where l is the element length, and hence

$$\begin{matrix} u \\ t \end{matrix} = b_0 + b_1 \sqrt{r} + b_2 r$$

The stress (traction) variation of $r^{-1/2}$ is achieved by simply multiplying the crack tip element coefficients by ($l\, r^{-1/2}$) :

$$t = c_0/\sqrt{r} + c_1 + c_2 \sqrt{r}$$

SIFs may be evaluated by a number of methods. Indirect methods may be used such by considering energy release rate or certain invariant integrals such as the J-integral. These methods appear to be computationally expensive with the BEM, and consequently we choose to use direct methods. There are two considerations which determine the type of boundary data used for direct computation of SIFs. Firstly, displacements are generally found to be more accurate than the corresponding stresses. Secondly, displacements on the crack surface are larger than those within the material. We therefore evaluate SIFs from crack openeing displacements.

Different estimates of SIF values are obtained by using different numbers of terms in the series expansions (4.1) and (4.2). The simplest estimate is obtained by using the first terms of the series expansion for displacements. We label points on the crack tip as in